Mechanistic Insights into the Role of Covalent Triazine Frameworks as Cathodes in Lithium-Sulfur Batteries

Erik Troschke[+],[a] Christian Kensy[+],[a, b] Frederik Haase,[c] Susanne Dörfler,[b] Yvonne Joseph,[d] Bettina V. Lotsch,[c] and Stefan Kaskel*[a, b]

This study illuminates the applicability of covalent triazine frameworks (CTFs) as a potential cathode material in lithium-sulfur (Li–S) batteries. A systematic synthesis protocol is applied to generate a set of model CTFs containing covalently bound sulfur with varying porosities and conductivities. An in-depth structural characterization reconsiders the bonding motif of sulfur within the pore system. The model materials are electrochemically evaluated in coin cells. The CTF cathodes exhibit practically no cycling performance as a result of active material loss in carbonate-based electrolyte ($\geq$200 mAh g_{sulfur}^{-1} after 200 cycles). Moreover, in ether-based electrolytes the differentiation between sulfur transformation on the surface of the conductive additive and the (semi-)conducting CTF matrix is hardly feasible. Based on these results, the influence of the CTF material and the conductive additive with respect to sulfur utilization are discussed, demonstrating the critical role of this class of materials for application in Li–S batteries.

1. Introduction

The increasing demand for efficient energy storage devices, in particular lithium-ion batteries (LIB), led to an intensive research towards innovative battery systems which could outperform the present battery technology in the near future. Such alternatives have to tackle multiple challenges; e.g. a high energy density and a good cycling stability of the battery device.[1] Considering also economic aspects, the combination of lithium and sulfur has emerged to be a very promising option, since elemental sulfur is a side product of chemical industry.[2] Additionally, sulfur provides a theoretical specific capacity of 1672 mA h g^{-1}, which is the highest of any solid cathode material.[3,4] For current prototype cells, practical values for the specific energy as high as 400 Wh kg^{-1} are achieved at significantly lower costs in regard to the active cathode material compared to state of the art LIBs.[5] Despite its remarkable benefits, this system currently presents some drawbacks like the extreme reactivity of the lithium anode leading to electrolyte depletion and cell dry out.[6] Furthermore, polysulfide intermediates are formed during reduction of elemental sulfur, which are well soluble in the widely used ether-based electrolytes. Thus, by diffusion ("shuttling") of these intermediates to the anode, a detrimental loss of active material from the cathode and an accompanied formation of an anodic Li_2S passivation layer is observed during cycling.[7]

Conductive host materials, such as porous carbons, have been proven to overcome the electrically insulating nature of sulfur by embedding the active material into the scaffold.[8] Although many efforts have been exploited to suppress the polysulfide shuttle using elaborated nitrogen-doped carbon materials,[9–11] metal oxide coating[12] or polymeric wrapping[13] of the composite material, the tendency of these intermediates to migrate within conventionally used ether-based electrolytes remains challenging. Moreover, carbonate-based electrolytes decompose upon reacting with those polysulfide species.[14] To avoid decomposition, one approach is to encapsulate sulfur into narrow and well-defined micropores of a porous carbon given that the overlapping of the Lennard-Jones potentials in these small pores lead to strong interaction between polysulfides and pore walls.[15,16,17] In such materials, the polysulfides are strongly adsorbed in the micropores, thus avoiding an irreversible reaction with the carbonates which consequently prevents irreversible decomposition of the electrolyte. Another innovative approach is the covalent bonding of sulfur to a conductive poly(acrylonitrile) (PAN) polymer.[18,19–22] The resulting sulfur rich polymer (SPAN) contains up to approx. 55 w% of

[a] Dr. E. Troschke,[+] C. Kensy,[+] Prof. Dr. S. Kaskel
Department of Inorganic Chemistry I
Technische Universität Dresden
Bergstraße 66, 01069 Dresden, Germany
E-mail: stefan.kaskel@tu-dresden.de
[b] C. Kensy,[+] Dr. S. Dörfler, Prof. Dr. S. Kaskel
Department of Chemical Surface and Battery Technology
Fraunhofer-Institute for Material and Beam Technology (IWS)
Winterbergstraße 28, 01277 Dresden, Germany
E-mail: stefan.kaskel@iws.fraunhofer.de
[c] Dr. F. Haase, Prof. Dr. B. V. Lotsch
Department of Nanochemistry
Max Planck Institute for Solid State Research
Heisenbergstraße 1, 70569 Stuttgart, Germany
E-mail: b.lotsch@fkf.mpg.de
[d] Prof. Dr. Y. Joseph
Department of Electronic and Sensor Materials
Technische Universität Bergakademie Freiberg
Gustav-Zeuner-Str. 3, 09599 Freiberg, Germany
E-mail: yvonne.joseph@esm.tu-freiberg.de
[+] These authors contributed equally.

Supporting information for this article is available on the WWW under https://doi.org/10.1002/batt.202000063

covalently bound sulfur after washing and shows almost complete sulfur utilization and stable cycling performance in a carbonate electrolyte, thus proving the absence of intermediate polysulfide species.[23,24]

Covalent triazine frameworks (CTF) recently attained great attention as another promising class of materials for Li/S battery applications.[25–27,28,29–31] CTFs are obtained by trimerization of aromatic nitriles under ionothermal conditions in molten $ZnCl_2$.[25,32,33] These porous organic polymers could possibly combine the benefits of both, the porosity of a carbonaceous host material as well as covalent bonding of the sulfur onto the matrix material.[25,34,35] CTFs benefit greatly from their modular design principle and allow for controlled porosity, chemical stability, and adsorption properties.[32,36] The latter allows for precise tailoring of the desired CTF material through the synthetic parameters, e.g. synthesis temperature or monomer size.[37] Furthermore, these nitrogen rich materials should be ideal candidates to prevent the polysulfide shuttle since they combine extended microporosity with polar surfaces.[29,31,38,39]

Previous works elucidates the synthesis of CTFs made from a nitrile precursor with a certain amount of embedded sulfur by adding sulfur prior to the CTF synthesis.[25,30,35] The resulting material presumably contains sulfur within the micropores of the CTF as well as covalently bound sulfur, which is connected to the polymeric backbone via C–H cleavage, thus replacing hydrogen by short chained sulfur. In the reported synthetic procedure, no washing step is carried out, thus the resulting material still contains large amounts of unreacted elemental sulfur at the inner and outer surface. Furthermore, it is well known that CTF materials are semiconductors as received at standard synthesis temperatures of 400 °C.[40] In consequence, large amounts of conductive additive (> 20 wt.%) were added to counterbalance the semiconductive nature of the CTF and realize the evaluation of the electrochemical performance in a sulfur cathode.[26,27,35] Moreover, a positive influence of the conductive additive on the sulfur utilization in an ether-based electrolyte cannot be excluded.

In order to improve the conductivity of CTF materials, See *et al.* presented an in-depth study which showcased the impact of the synthesis temperature on the electrochemical behavior in lithium salt and carbonate-based electrolytes. They pointed out that synthesis temperatures above 500 °C are crucial to induce electrical conductivity in the CTF material.[41] Thereby, the well-defined polymers are partially decomposed, creating N-containing amorphous carbon rather than a defined CTF material. In addition, these materials were found to perform similar to super-capacitor materials but showed redox activity in contrast to a pure carbon material.[42]

In the following, we reinvestigate the mechanistic role of covalent triazine frameworks as host materials for covalently bound sulfur. By selecting two representative model CTFs we study their ability to bind sulfur as a function of monomer size and three different synthesis temperatures. Consequently, we compare their electrochemical performance in two different electrolytes: a standard ether-based electrolyte for Li–S cathodes and the carbonate-based electrolyte LP30. Based on these results, the influence of the synthesis temperature on porosity, conductivity, amount of covalently bound sulfur, and its utilization in the respective electrolytes indicates that the hitherto reported beneficial role of covalently bound sulfur in CTFs is overestimated.

2. Results and Discussion

Cathode materials require a critical conductivity for battery applications. However, such conductivity is not achieved in CTFs synthesized at only 400 °C as these are known to be large band gap semiconductors with low charge carrier mobilities.[40] In order to obtain conductive materials, all CTF syntheses were conducted at 400 °C in combination with an additional inert heating step at 500 °C, 600 °C and 700 °C, respectively. In consequence, the networks partially carbonize depending on the pyrolysis temperature. For our study, we decided to synthesize two different model CTFs made from 1,4-dicyanobenzene (CTF-Mono) and 4,4′-dicyano-1,1′-biphenyl (CTF-Bi) (see Scheme 1).

The CTF-Bi system was intended as a system with an enhanced amount of potential sites for covalent sulfur bonding compared to CTF-Mono, due to the increased number of C–H groups in the precursor. For CTF-Mono, as expected, higher reaction temperatures of the polymers are accompanied by a large increase of porosity as determined by nitrogen physisorption measurements at 77 K (see Figure 1, a more detailed explanation of this phenomenon is given later). All three materials synthesized at varying temperatures show high gas uptake in the low relative pressure range, reflecting a high micropore volume. Thus, high specific BET surface areas of 2120 $m^2 g^{-1}$ (CTF-Mono_500), 2730 $m^2 g^{-1}$ (CTF-Mono_600) and 2780 $m^2 g^{-1}$ (CTF-Mono_700) were determined. In addition, enhanced mesoporosity was observed for the materials synthesized at 600 °C and 700 °C, respectively. As a consequence, CTF-Mono_600 and CTF-Mono_700 show total pore volumes of 2.10 $cm^3 g^{-1}$ and 2.20 $cm^3 g^{-1}$, which significantly exceed the pore volume

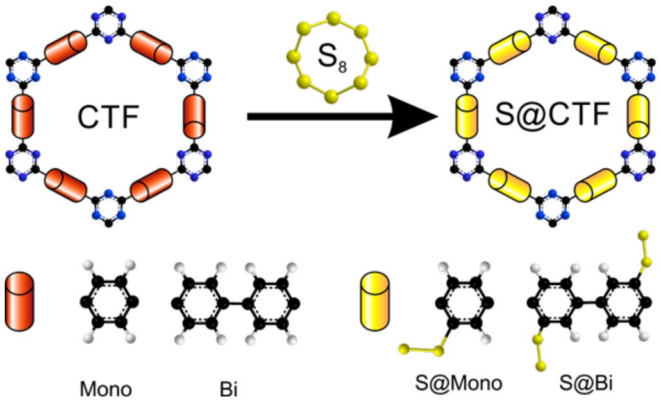

Scheme 1. Synthesis principle of the CTF-sulfur composite materials by using two types of linker molecules.

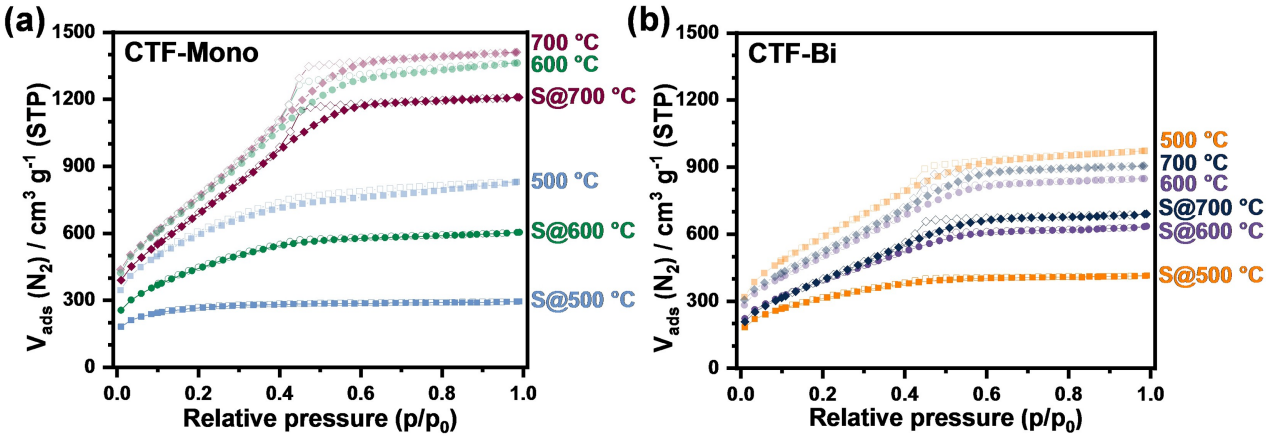

Figure 1. Nitrogen physisorption isotherms (77 K) of CTF materials synthesized at different temperatures and derived materials containing covalently bound sulfur obtained from a) 1,4-dicyanobenzene (CTF-Mono) and b) 4,4′-dicyano-1,1′-biphenyl (CTF-Bi).

of CTF-Mono_500 (1.30 $cm^3 g^{-1}$). In contrast, there is no pronounced impact of the reaction temperature on the porosity of the CTF-Bi materials. Interestingly, CTF-Bi_500 exhibits the highest BET surface area (2130 $m^2 g^{-1}$) of all three samples. This effect might potentially be attributed to a reorganization of the polymeric scaffold during the transformation and graphitization processes leading to a competing reduction in porosity of the samples treated at 600 °C and 700 °C as an effect of elevated reaction temperatures.[46] Moreover, at these temperatures enhanced carbonization reactions and even cycloaddition reactions of the biphenyl can occur.

In consequence, mesopores are created at the expense of micropores, thus causing decreased micropore content (see Supporting Information, Section 3 for pore size distributions and 4 for pore volumes). However, also CTF-Bi_600 and CTF-Bi_700 show high specific surface areas of 1800 $m^2 g^{-1}$ and 1870 $m^2 g^{-1}$, respectively (see Table 1).

The next target was to covalently tether sulfur onto the CTF materials. Thus, the activated samples were thoroughly mixed with an excess of sulfur (15 mass eq.) in a ball mill and transferred into an argon purged tubular furnace. In order to impregnate the samples with sulfur, the samples were kept at 155 °C given the fact that sulfur has its lowest viscosity at that temperature. To reach covalent bonding, the temperature was subsequently raised to 350 °C to induce substitution of hydrogen against sulfur. To remove residual elemental sulfur potentially remaining within the materials after the synthesis, the samples were carefully washed by means of two successive Soxhlet extractions (toluene and THF). To investigate how sulfur bonding affects the porosity, nitrogen physisorption measurements were conducted in order to compare the parent material and the sulfur loaded CTFs. The isotherms of all sulfur loaded CTF samples (S@CTF-Mono and S@CTF-Bi) reveal a global decrease of specific surface area and total pore volume (see Figure 1 and Table 1). This trend indicates that sulfur within the pore system strongly influences the porosity. In order to exclude a loss of porosity due to mechanical stress caused by ball milling, CTF-Bi_500 was mixed with sulfur (following the same procedure as used for all samples) as a reference sample. After Soxhlet washing with toluene, no loss of porosity could be detected, thus indicating an intact pore system (see Supporting Information, Figure S5).

To gain further insight we employed Quenched Solid Density Functional Theory (QSDFT) to analyze if the sulfur is preferentially located in the micro- or mesopores of the parent materials. Comparing the respective micropore- (V_{micro}) and mesopore volumes (V_{meso}) prior to and following sulfur treatment verifies that both pore types are filled – in all cases the micropore as well as the mesopore volume of the S@CTF samples show a decrease.

For example, CTF-Mono_500 has a micropore volume of $V_{micro} = 0.76$ $cm^3 g^{-1}$ and mesopore volume of $V_{meso} = 0.51$ $cm^3 g^{-1}$, respectively. For the sulfur treated sample S@CTF-

Table 1. Porosity data of all CTF samples and their sulfur-treated analogues (from nitrogen sorption at 77 K).[a]

Sample	SSA [$m^2 g^{-1}$]	V_{micro} [$cm^3 g^{-1}$]	V_{meso} [cm3 g^{-1}]	V_{tot}[b] [$cm^3 g^{-1}$]	Sample	SSA [$m^2 g^{-1}$]	V_{micro} [$cm^3 g^{-1}$]	V_{meso} [$cm^3 g^{-1}$]	V_{tot}[b] [$cm^3 g^{-1}$]
CTF-Mono_500	2120	0.76	0.51	1.28	CTF-Bi_500	2130	0.65	0.85	1.50
CTF-Mono_600	2730	0.76	1.34	2.10	CTF-Bi_600	1800	0.53	0.77	1.30
CTF-Mono_700	2780	0.75	1.43	2.18	CTF-Bi_700	1870	0.55	0.84	1.39
S@CTF-Mono_500	970	0.39	0.06	0.45	S@CTF-Bi_500	1130	0.41	0.23	0.64
S@CTF-Mono_600	1620	0.58	0.35	0.93	S@CTF-Bi_600	1430	0.45	0.53	0.98
S@CTF-Mono_700	2700	0.72	1.15	1.87	S@CTF-Bi_700	1475	0.43	0.60	1.07

[a] Abbreviations: SSA (specific surface area); V_{micro} (micropore volume); V_{meso} (mesopore volume); V_{tot} (total pore volume). [b] Determined at $p/p_0 = 0.95$.

Mono_500, the values drop down to $V_{micro} = 0.39\ cm^3\ g^{-1}$ and $V_{meso} = 0.06\ cm^3\ g^{-1}$. Moreover, we investigated the percental deviation of the respective micropore and mesopore volume after sulfur treatment for the samples synthesized from the same monomer but at different temperatures. To showcase this effect, the respective values of S@CTF-Mono samples are applied. For CTF-Mono_500 a drop of the micropore volume of $\Delta V_{micro} = 49\%$ and for the respective mesopore volume of $\Delta V_{meso} = 88\%$ was found. Considering the samples S@CTF-Mono_600 and S@CTF-Mono_700, our data show that the percental deviation decreases with higher temperatures. At 600 °C, a drop of $\Delta V_{micro} = 24\%$ and $\Delta V_{meso} = 73\%$ is observed. Even lower values of $\Delta V_{micro} = 5\%$ and $\Delta V_{meso} = 19\%$ were determined for the S@CTF-Mono_700 sample. In accordance with these values, also the S@CTF-Bi samples show comparable trends. Based on these findings, a slight preference of sulfur bonding for mesopores was observed.

Elemental analysis was conducted to further investigate the amount of covalently bound sulfur within the CTF materials (see Figure 2). Since higher synthesis temperatures induce more carbonization of the CTF materials, increased carbon/hydrogen and carbon/nitrogen ratios are expected for samples synthesized at 600 °C and 700 °C. The former should result in less covalently bound sulfur, since the number of C–H binding sites will be reduced. In agreement with this hypothesis, we found decreasing amounts of sulfur progressing from lower to higher synthesis temperatures. S@CTF-Mono_500 shows a total sulfur content of ca. 29 w%, whereas S@CTF-Mono_600 and S@CTF-Mono_700 show values of ca. 12 w% and 9 w%, respectively. Also for the S@CTF-Bi samples, the values decrease with higher temperatures from 34 w% to 17 w% and 11 w% (see Supporting Information, Table S1).

Powder X-ray diffraction (PXRD) revealed no additional reflections assignable to elemental sulfur (here referenced to α- and β-sulfur)[9,47] within the sulfur treated samples (see Figure 3a/3b). All samples remained amorphous after sulfur bonding (see Supporting Information, Section 6 for PXRD data of other samples). Thus, three potential conclusions can be drawn from these findings. Either no elemental sulfur is present within the samples as a separate crystalline phase or sulfur is finely dispersed at the nanometer scale or in an amorphous polymeric form. All of which would preclude detection via the PXRD technique.

The bonding of sulfur within the CTFs was probed with the help of X-ray photoelectron spectroscopy (XPS) (see Figure 3c/3d). For better understanding, all trends are discussed with regard to the CTF-Mono_600 and CTF-Bi_600 samples and their sulfur treated analogues. Survey XPS spectra comparing the parent material and its sulfur treated counterpart clearly reveal the presence of sulfur in the S@CTF samples (see Supporting Information, Figure S8/S9). In addition, carbon, nitrogen, traces of residual zinc (Zn 2p: 1022 eV), and chlorine (Cl 2p: 199 eV) can be observed.[48] Interestingly, the peak for oxygen is much more pronounced in the sulfur containing samples S@CTF-Mono_600 and S@CTF-Bi_600. This observation can be attributed to a potential oxidation of sulfur atoms towards SO_x species which could take place upon exposure to ambient conditions during washing. High resolution S 2p spectra show that there are various sulfur environments within the samples. The main peak with a binding energy of 163.30 ± 0.10 eV ($2p_{3/2}$) and a shoulder at a binding energy of 164.40 ± 0.10 eV ($2p_{1/2}$) can be referred to as a C–S or S–S bonding motif.[49,50] Since the XPS data do not allow for a distinction of these species, the results need to be considered in combination with the findings gained from other methods. The PXRD data reveal no elemental sulfur, thus strengthening the hypothesis of covalently bound or polymeric sulfur.[48] Other peaks were observed at binding energies of 165.00 ± 0.10 eV ($2p_{3/2}$; sulfoxides), 167.20 ± 0.10 eV ($2p_{3/2}$; sulfones) and 168.30 ± 0.10 eV ($2p_{3/2}$; sulphates), which suggests the existence of oxidized (terminal) sulfur atoms.[49,50] When taking also into account the C 1s XPS data (see Supporting Information, Figure S13/S16 and Table S2) of CTF-Mono_600, CTF-Bi_600 and their sulfur treated analogues, an increase of the peak area of the C=N or C–S peak (BE = 285.70 ± 0.30 eV) for S@CTF-Mono_600 and S@CTF-Bi_600 becomes apparent. These findings indicate the generation of C–S species in the

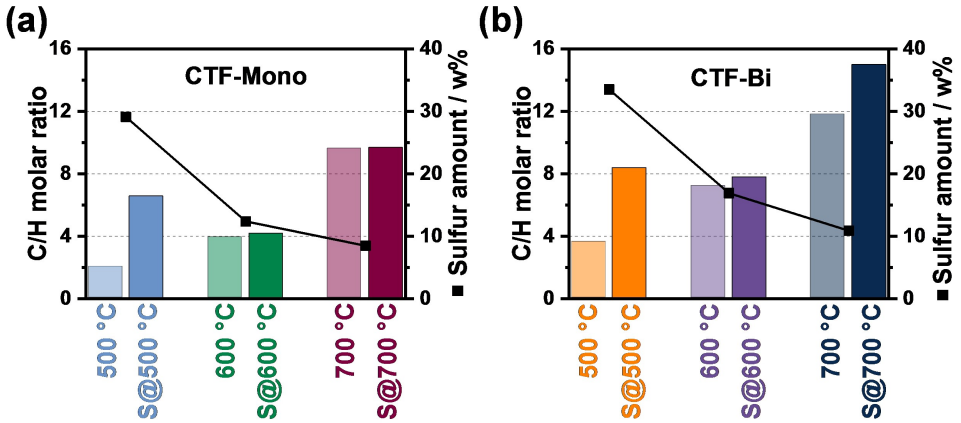

Figure 2. Elemental analysis and the respective C/H molar ratios of CTF-Mono samples (a) and CTF-Bi samples (b) received at different temperatures. Sulfur content with respect to the synthesis temperature for S@CTF-Mono (a) and S@CTF-Bi (b) samples.

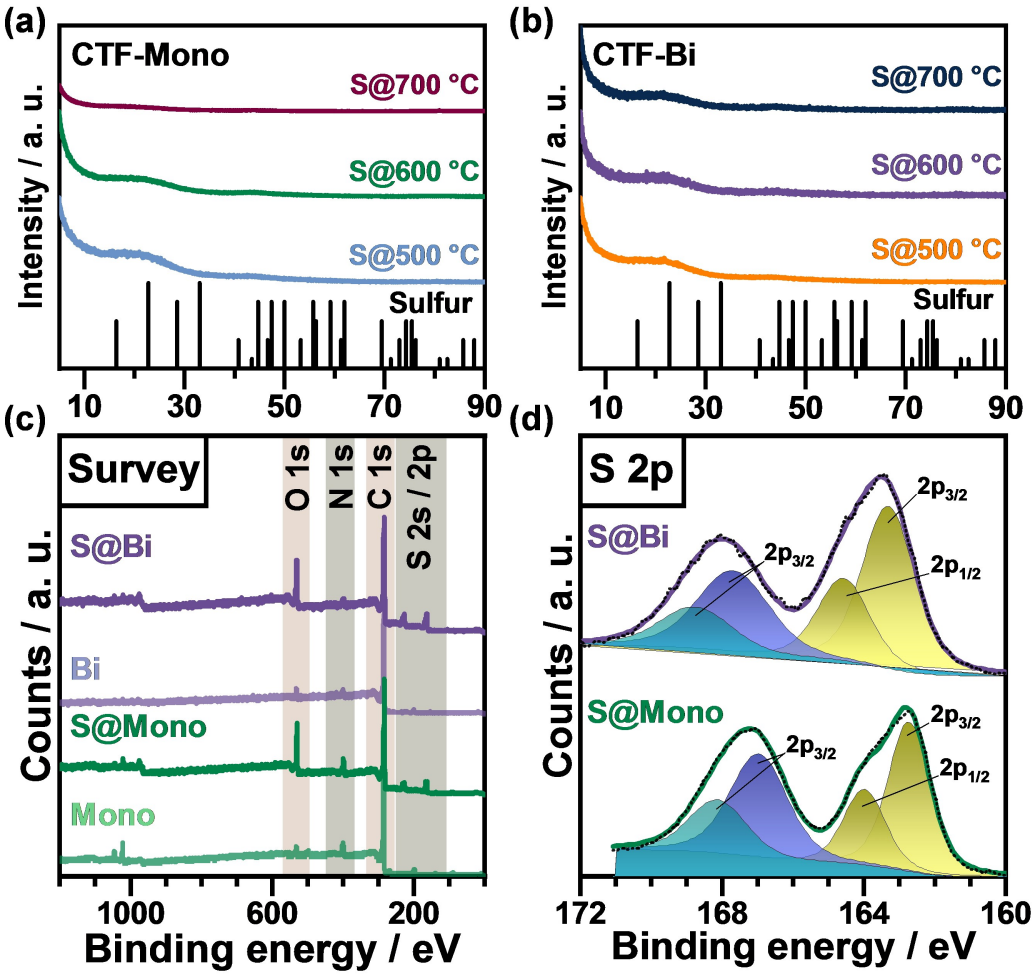

Figure 3. Powder X-ray diffraction data of a) S@CTF-Mono, b) S@CTF-Bi and sulfur as reference. X-ray photoelectron spectroscopy survey of CTF and S@CTF samples received at 600 °C (c), and high resolution S 2p spectra of S@CTF-Mono_600 and S@CTF-Bi_600 (d). For clarity, the peak fit function was obtained by adding $p_{1/2}$ and $p_{3/2}$ components with respective binding energy distance and intensity ratio resulting in an asymmetrical fit function comprising both spin-orbit split signals.

sulfur treated materials. Thus, the existence of short sulfur chains which most likely contain differently oxidized terminal atoms may be hypothesized (see Supporting Information, Section 7 for XPS data of other samples).

Fourier transform Infrared spectroscopy (FT-IR) displays a high degree of carbonization for all samples which is reflected by very broad and lack of well resolved peaks. In spite of that, an additional broad vibration at approximately 1060 cm^{-1} is observed for all sulfur treated samples, which may be assigned to C=S stretching modes (see Supporting Information, Section 8 for FT-IR data of all samples).[49,51] In line with these findings, the intensity of the new vibration decreases when comparing the samples received at lower reaction temperatures (thus, containing more sulfur) and the high temperature samples (containing less sulfur).

Scanning electron microscopy (SEM) revealed a rough surface, showing no distinct difference between the parent materials and their sulfur treated analogues (see Supporting Information, Section 9 for SEM of all samples).

After the structural evaluation, the materials were characterized in terms of their electrochemical properties. The main question to be clarified was how S@CTF cathodes perform compared to materials like SPAN and showing reversible sulfur utilization in carbonate-based electrolyte without irreversible electrolyte depletion by reaction of polysulfides with the carbonates.[21,22,52] As carbonate-based electrolyte LP30 was used. Additionally, the S@CTF cathodes were tested in ether-based electrolyte (1 M LiTFSI in dimethoxyethane (DME) and 1,3-dioxolane (DOL) 1:1 by volume) in order to analyze the electrochemical reaction mechanism of the sulfur species and to evaluate the results with respect to the literature.[4,53,54] For the comparison of the different model CTF materials, the two electrolyte systems were studied in the same potential range. The S@CTF electrodes for the galvanostatic measurements were generated by a solvent-free dry process as described elsewhere, with a slightly changed weight ratio (S@CTF: conductive additive:binder = 75:20:5).[44] Higher annealing temperatures lead to fewer potential anchoring sites for sulfur

bonding, and hence, to reduced cathode sulfur loadings ranging from 2.50–5.00 $mg_{electrode}$ cm^{-2}.

Figure 4 reveals the cycling performance and the discharge voltage profiles of the S@CTF-Bi_500 cathodes for both electrolyte systems. For the carbonate-based electrolyte a discharge capacity of 420 mAh g_{sulfur}^{-1} was achieved in the first cycle (see Figure 4a). The corresponding discharge voltage curve (see Figure 4c) shows only one plateau at 2.49 V (vs. Li/Li^+) originating from the formation of longer polysulfide intermediates (Li_2S_n, $n=6$–8)[55], and subsequently, the discharge curve drops in the successive cycles. Thus, after the first cycle, the capacity decreases to the value of the unloaded CTF material (see Supporting Information, Figure S41). It is known that organic carbonate-based electrolytes irreversibly react with freely dissolved lithium polysulfides depending on the porous structure of the carbon material.[14] Regarding the latter, micropores act as an energetic well due to the overlapping Lennard-Jones potentials and hence, an increased adsorption potential for small sulfur species is observed.[15,39] Shorter chain sulfur intermediates (S_{2-4}) confined in micropores are understood to not undergo irreversible reactions with carbonates.[15,17,56] Nevertheless, CTF materials exhibit mesopores as well (see Figure 1 and Table 1) and thus, during the first discharge process longer polysulfides were generated and react with the carbonate molecules by nucleophilic attack. These side reactions are also responsible for a coulombic efficiency (CE) higher than 100%, due to the irreversible active material loss during cycling. The discussed observations give rise to the conclusion that CTF materials with covalently bound sulfur seem to follow a different electrochemical conversion mechanism compared to SPAN in carbonate-based electrolyte.

In contrast to the carbonate-based electrolyte, the S@CTF-Bi_500 cathode showed a moderate cycling performance in the ether-based electrolyte (see Figure 4b). The initial capacity of 1053 mAh g_{sulfur}^{-1} decreased to a value of 356 mAh g_{sulfur}^{-1} after 200 cycles. In the first 10 cycles, the CE dropped from 116% to 85%. The drastic decrease is reasoned by the lack of $LiNO_3$ as an electrolyte additive, which typically promotes the formation of a solid electrolyte interface (SEI).[57–59] $LiNO_3$ is known to be decomposed below 1.80 V (see Figure S39) and hence, it was not added to the electrolyte in order to compare the results with the carbonate-based electrolyte and studies with SPAN where the cathodes were cycled between 1.00–3.00 V.[20–22,57,60] Without $LiNO_3$, a less stable SEI is formed at the Li anode leading to continuous electrolyte decomposition and loss of active material at the anode due to the polysulfide shuttle.[58–60] After 48 cycles, a SEI seems to be generated (CE ≈ 100%), and the S@CTF-Bi_500 material shows a nearly constant capacity retention. Interestingly, a small plateau/shoulder at 2.35 V is observed at the discharge slope that might be attributed to the direct reduction of dissolved S_8, given that this shoulder was also described for SPAN materials (see Figure 4d).[19,20,22] During the first discharge, the sulfur that is not directly bound to

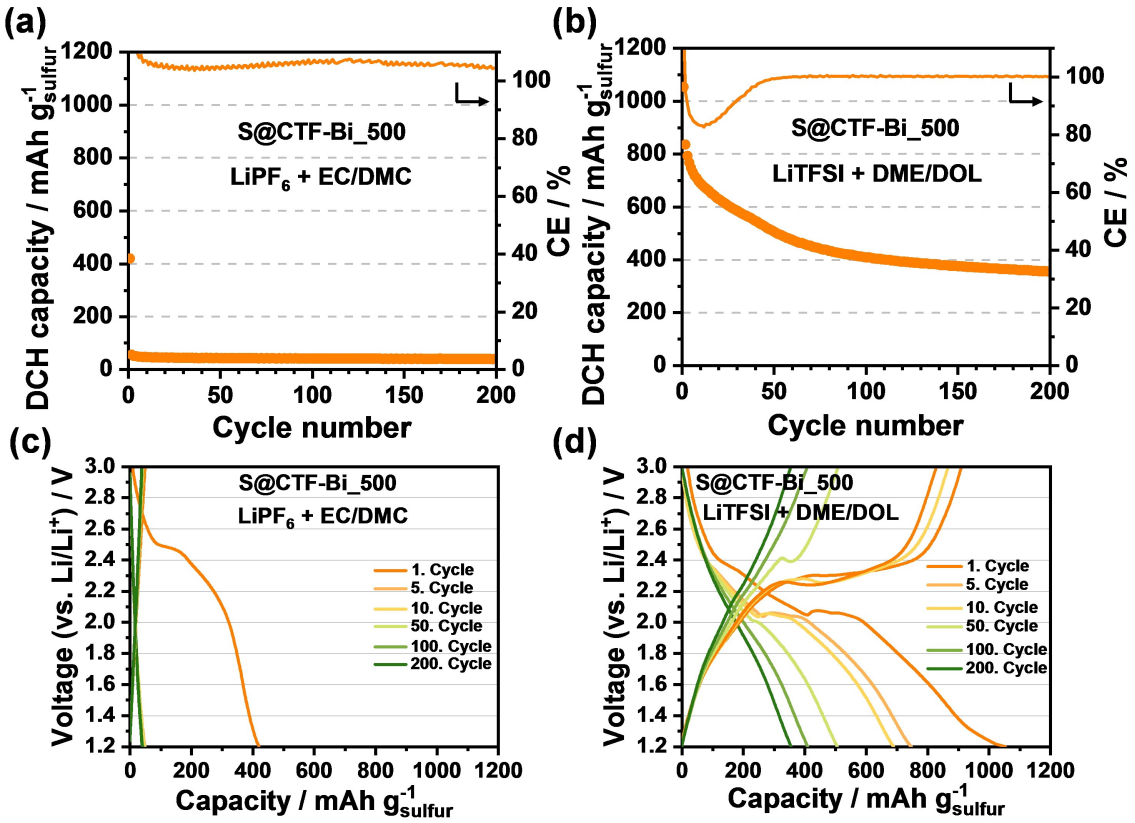

Figure 4. Galvanostatic cycling and discharging capacities of the S@CTF-Bi_500 sample in carbonate-based (a) and ether-based (b) electrolyte at C/10 and the corresponding voltage profiles in carbonate-based (c) and ether-based electrolyte (d).

carbon but to other sulfur species (e.g. R-S-S_x) is first reduced and released from the polymer backbone.[20]

In contrast, the discharge curves obtained in ether-based electrolytes show a quite pronounced second plateau at 2.10 V that clearly diminishes after 50 cycles, as expected for DME/DOL-based electrolytes without $LiNO_3$ addition (see Figure 4d). Additionally, the drop of the slope after the second plateau is less steep compared to conventional carbon-sulfur cathodes and previous CTF cathode results.[11,35] In combination with the low CE in the first 50 cycles and lack of $LiNO_3$, the polysulfide species diffuse preferentially to the (almost unprotected) Li anode. Hence, the desired formation of the discharged species Li_2S at cathode side is hindered.[6] As a result, a less pronounced second plateau in the voltage profile is observed with increasing cycle number.

In contrast to previous CTF applications in Li–S batteries, no confinement of the sulfur, but a drastic loss of capacity due to active material loss was observed.[25,35] Therefore, the electrochemical performance of the S@CTF cathodes with ether-based electrolytes needs a critical evaluation, especially in light of the fact that a considerable amount of conductive additive (in our study 20 wt.% of Ketjenblack) has been utilized. This significant content of conductive additive can influence the cell performance and sulfur utilization. During cycling the generated polysulfides can diffuse out of the CTF matrix, which acts as a kind of polysulfide and electrolyte storage reservoir for the more conductive carbon black sites. Thus, the dissolved polysulfide intermediates could be reduced at the carbon black particles due to the higher conductivity. We believe that the electron transfer, and thus the electronic conductivity of the cathode material in general plays a key role for the sulfur reduction mechanism, as discussed for standard carbon-sulfur composite cathodes in DME/DOL-electrolyte.[53,61,62] Unfortunately, previous publications about CTF materials for Li–S application do not differentiate between sulfur utilization via the conductive additive versus the actual CTF matrix.[25,30,35,63]

In order to uncover the effect of host conductivity, subsequently the influence of the synthesis temperature of the CTF materials on the sulfur utilization was investigated. A reliable assessment of CTFs as potential cathode material is challenging, since a large amount of conductive additive is added in most references prior to the electrode preparation, most probably in order to realize appropriate sulfur utilization.[26,30,35,63] In order to reveal the impact of the CTFs' conductivity, resistivity measurements of sulfur loaded materials and the unloaded CTF-1 have been performed (see Supporting Information, Section 10). The results reveal that the specific resistivity of all produced S@CTF samples is far smaller (by 6 orders of magnitude: MΩ vs. Ω) as compared to unloaded and previous published CTF-1 obtained at 400 °C.[25,35]

Moreover, sulfur is electrically insulting with an electrical conductivity of 5×10^{-30} S cm^{-1} (at 25 °C).[64] Hence, it can be concluded that a synthesis temperature of at least 500 °C is required to synthesize intrinsically conductive CTF materials. In addition, lower specific resistance values are achieved for higher synthesis temperatures due to the higher carbonization degree of the CTFs. To verify the influence of the synthesis temperature all S@CTF materials were investigated in both, carbonate- and ether-based, electrolytes. In analogy to previous findings, the discharge slopes in carbonate-based electrolyte showed similar behavior and irreversible capacity loss in the first cycle as the aforementioned S@CTF-Bi_500 (see Figure 4a/4c, and Supporting Information, Section 10 for discharge capacities of the other samples).

The corresponding results with ether-based electrolyte are discussed in the following (see Figure 5): After 200 cycles, S@CTF-Mono_700 show the highest discharge capacity of 1046 mAh g_{sulfur}^{-1} as compared to S@CTF-Mono_600 and S@CTF-Mono_500, with 779 mAh g_{sulfur}^{-1} and 387 mAh g_{sulfur}^{-1}, respectively. In order to corroborate the conductivity influence a S@CTF-1 composite as reference was analyzed under same conditions and exhibited only a moderate sulfur utilization as well as cycle performance with lower discharge capacities (see Figure S40) despite the sulfur loading was rather low (13.5 wt %). Also for the S@CTF-Bi cathodes, the discharge capacities decrease with lower synthesis temperature. The value of the first cycle discharge capacity of the S@CTF-Mono_700 cathode (2582 mAh g^{-1}) was much higher than the theoretical specific

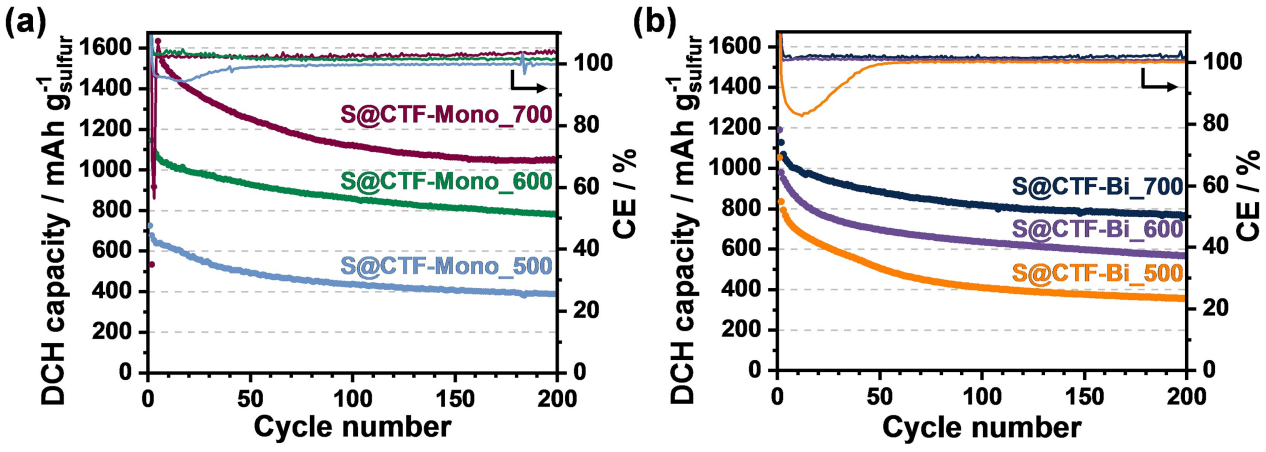

Figure 5. Galvanostatic cycling and discharging capacities of the different S@CTF-Mono (a) and S@CTF-Bi (b) cathodes in ether-based electrolyte at C/10.

capacity of sulfur (1672 mAh g^{-1}). This phenomenon was reported for SPAN with ether-based electrolyte as well.[20] At the beginning of discharge, the formation of C-S_x-SLi species is more favored than the formation of Li_2S. The C-S_x-SLi moieties are reduced to Li-thioketones and the further reduction of the generated π-system led to a capacity increase in the last part of discharge.[20,22,23]

Another reason could be the decreased sulfur content with higher temperatures, for 600 °C: 9–12 w% and for 700 °C: 6–8 w % sulfur in the cathode and thus, the error in calculating the theoretical capacity continuously increases with lower amounts of sulfur and influences the utilization of active material drastically. Therefore, these high capacity values are prone to errors and should be considered cautiously.

Furthermore, the different CTF structures (CTF-Mono, CTF-Bi) and hence, different amounts of potential sulfur anchoring sites are electrochemically compared (see Figure 5). After 200 cycles the S@CTF-Mono cathodes (500 °C: 388 mAh g_{sulfur}^{-1}, 600 °C: 779 mAh g_{sulfur}^{-1}, 700 °C: 1046 mAh g_{sulfur}^{-1}) exhibit higher capacities in contrast to the S@CTF-Bi-cathodes (500 °C: 356 mAh g_{sulfur}^{-1}, 600 °C: 566 mAh g_{sulfur}^{-1}, 700 °C: 767 mAh g_{sulfur}^{-1}). This effect could be occurred by the lower amount of anchoring sites and therefore, lower overall sulfur loadings. It is known from the literature that lower sulfur loadings can be utilized more efficiently.[61] Moreover, the as mentioned estimated error for the electrode capacities also increases with lower sulfur contents. However, the initial capacity of S@CTF-Bi_500 (1054 mAh g_{sulfur}^{-1}) was higher compared to S@CTF-Mono_500 (725 mAh g_{sulfur}^{-1}). This result can be attributed to higher amount of mesopores of S@CTF-Bi_500 material. Hence, the created polysulfides diffuse more easily out of the CTF matrix and seem to be enhanced utilization at the carbon black particles. Moreover, both samples show the already described degradation step due to SEI formation for the first 50 cycles. This effect can also be attributed to the sulfur contents of these cathodes (22 w% for S@CTF-Mono cathode and 26 w% for S@CTF-Bi_500 cathode) and the utilized electrolyte amount. The concentration of dissolved polysulfides is higher compared to CTF cathode with lower sulfur contents and hence, their influences on side reactions, e.g. SEI formation or depletion by the lithium anode have an increased impact on the cell performance. However, the CE degradation is more pronounced for the S@CTF-Bi_500 sample which could be an effect of the higher porosity and polysulfide accessibility.

Summarizing, the monomers and their amount of possible anchoring sites for sulfur species exchange have far smaller influence on electrochemical performance than the CTF synthesis temperature. Our findings suggest that the sulfur conversion mechanism is more significantly affected by the highly conductive carbon black additive and its redox active surface sites rather than the CTF material. The role of the CTF scaffold can thus be interpreted primarily as a polysulfide/electrolyte host.[26,27,29]

3. Conclusions

Our critical reinvestigation of covalent triazine frameworks as host materials for covalently bound sulfur reveals that previously emphasized benefits are likely overrated. The analysis of two model CTFs to study their ability to bind sulfur as a function of monomer size and three different synthesis temperatures led to materials with varying conductivities and porosities. The model materials were investigated applying a comparative electrochemical characterization in half-cells vs. Li/Li^+ with two different electrolyte systems. The discussed observations give rise to the conclusion that CTF materials with covalently bound sulfur seem to follow a different conversion mechanism compared to SPAN in carbonate-based electrolyte. In contrast to SPAN cathodes, already the first cycle revealed a drastic loss of capacity. Thus, no stable cycling performance was observed, which is most probably caused by a loss of active material.

Consequently, also the cycle performance of the S@CTF materials in ether-based electrolyte was critically reinvestigated. The influence of the amount of covalently bound sulfur, and its utilization were analyzed. We observed that the monomeric subunits of the framework and the abundance of anchoring sites for sulfur species exchange are less influential for the electrochemical performance than the synthesis temperature and herewith affected conductivity of the CTF scaffold. In particular, the presented results suggest that the conversion mechanism most probably proceeds via the highly conductive sites of the carbon additive rather than the CTF structure which only acts as a polysulfide/electrolyte host. Hence, the differentiation between sulfur transformation on the surface of the conductive additive versus the (semi-) conducting CTF matrix is hardly feasible. Most importantly, our survey provides new insights into the sulfur utilization of covalently bound sulfur at CTF materials, which puts previously reported results into perspective. Enhancing the intrinsic electrical conductivity of porous organic frameworks and establishing protocols for the defined functionalization with redox-addressable sulfur species is an important prerequisite for the deliberate exploration and understanding of this material class in Li–S batteries in future.

Experimental Section

Materials and reagents

Zinc chloride (ABCR, anhydrous, 98%) was stored in a glovebox and used as received. 1,4-Dicyanobenzene (Sigma Aldrich, 98%) and 4,4′-dicyano-1,1′-biphenyl (ABCR, 98%) were dried at 50 °C under vacuum prior to handling it in a glovebox. Sulfur (Grüssing, 99.5%) was used as received.

General Methods

Elemental analysis was carried out on a *vario* MICRO cube Elemental Analyzer by Elementar Analysatorsysteme GmbH in

CHNS modus. The samples were activated at 150 °C prior to the measurement.

Nitrogen physisorption measurements were performed at 77 K on a Quadrasorb (Quantachrome Instruments) using high purity gas (N_2: 99.999 %). Specific surface area (SSA) were calculated using the equation from Brunauer, Emmett and Teller (BET) in a relative pressure range that fits to the consistency criteria proposed by Rouquerol and Llewellyn.[43] Pore size distributions were calculated using the Quenched Solid Density Functional Theory (QSDFT) method for carbon (slit pores, equilibrium kernel) using the adsorption branch. Ultramicropore volumes were calculated from the cumulative pore volumes at a pore diameter of less or equal to 0.70 nm. Supermicropore volumes were determined by subtracting the respective micropore volume from the cumulative pore volume at a pore diameter of 2 nm. Mesopore volumes were determined by subtracting the respective micropore volume from the cumulative pore volume at a pore diameter of 26 nm. Total pore volumes were calculated at a relative pressure of $p/p_0 = 0.95$. Prior to physisorption experiments, samples without sulfur were activated at 423 K and samples with sulfur at 293 K for 24 h under vacuum (prior to physisorption experiments, all samples were dried at 423 K under vacuum).

Powder X-ray diffraction (PXRD) patterns were collected in transmission geometry (MYTHEN 1 K detector) with a STOE STADI P diffractometer operated at 40 kV and 30 mA with a Ge monochromator using Cu–Kα1 radiation.

XPS measurements were conducted with a Theta Probe photoelectron spectrometer (Thermo Scientific). The spectrometer was equipped with a monochromatic Al Kα X-ray source of 100 W at 15 kV. The kinetic energy of photoelectrons was determined with hemispheric analyzer set to pass energy of 200 eV for wide-scan spectra and 50 eV for high-resolution spectra. High-resolution spectra were deconvoluted by means of the Casa XPS deconvolution software. A linear spectrum background was subtracted. The deconvolution of spectra was performed using a mixed Gauss-Lorentz function where the Lorentzian contribution was set to 30 % and a full width at half maximum that was kept constant within one sample. Free parameters of component peaks were their binding energy (BE) and height. Quantitative elemental compositions were determined from the integrals of the Gauss-Lorentz fit functions.

Scanning electron microscope images were obtained using a Hitachi SU8020 SEM equipped with a secondary electron (SE) detector. Prior to the measurement the samples were prepared on an adhesive carbon pad and sputtered with gold to obtain the necessary electron conductivity.

A Nabertherm P330 oven was used as heating device for all CTF syntheses. For covalent attachment of sulfur, an argon purged tubular furnace (Gero 30–3000 °C) equipped with a quartz tube was used.

Fourier transform infrared spectroscopy was performed on a Bruker Vertex 70 in the range from 4000 to 600 cm^{-1} (resolution 2 cm^{-1}, ATR).

Specific resistivity and conductivity of CTF materials was determined for pellets (diameter: 1 cm) after compression in a hollow cylinder using a punch press (max. p = 2 t). The punch as well as the bottom of the cylinder are the measurement electrodes. The electric resistivity was determined during the compression process between these two electrodes. The specific resistivity of the CTF materials was derived from the measured resistivity at p = 2 t, the sample weight and the cell diameter.

General synthesis procedures for CTFs and S@CTF materials

CTF syntheses were performed in ampoules which were prepared under inert atmosphere (in a glovebox). In a typical synthesis, 500 mg of the respective monomer and 5 eq. $ZnCl_2$ were mixed by grinding and transferred into quartz ampoules. The ampoules were sealed under vacuum and heated (for temperature program see Supporting Information). The ampoules were then cooled down to room temperature and opened. The reaction product was subsequently ground and then stirred in 1 N HCl for 24 h at 60 °C. The sample was then washed thoroughly with water, *N*,*N*-dimethylformamide and acetone to remove residual salt and organic impurities. After washing, the resulting black powder was dried at 150 °C. The CTFs were activated at 150 °C under vacuum and mixed with the 15-fold amount (weight) of sulfur in a ball mill. The resulting homogeneous mixture was transferred in a quartz boat in a horizontal tubular furnace and purged at 60 °C under flowing argon. The temperature was increased to 155 °C (60 K/h heating rate) and maintained there for 3 h. Then the temperature was raised to 350 °C (100 K/h heating rate) and kept for 3 h. After cooling down, the resulting material was washed via Soxhlet extraction with toluene and THF for 24 h, respectively. The samples were dried at 70 °C in an oven and then at 150 °C under vacuum.[44]

CTFs and S@CTF cathode preparation

CTF cathodes were prepared from S@CTF as well as CTF material similar to a solvent-free roll press procedure reported elsewhere.[45] The S@CTF/CTF material were mixed with a carbon black (Ketjenblack EC600JD, AkzoNobel) and poly(tetrafluoroethylen) (PTFE) binder in a slightly changed weight ratio of 75:20:5. After homogenization and intensive grinding, electrode sheets were prepared using shearing forces. The free-standing electrode films were then laminated onto a primer-coated aluminium current collector for electrochemical characterization. For coin cell tests, circular electrodes with a diameter of 12 mm were punched out with active mass loadings of 2.50–5.00 $mg_{electrode}cm^{-2}$ and a thickness of 100 ± 10 μm.

Electrochemical characterization

For electrochemical characterization CR2016 coin cells were assembled in an Argon-filled glove box (MBraun, conditions: < 0.1 ppm O_2 and H_2O) by stacking the CTF/S@CTF cathode, a Celgard 2500 separator (diameter: 19 mm, thickness: 25 μm) and an elemental lithium chip (diameter: 16.50 mm, thickness: 250 μm). Before sealing an appropriate amount (30 μl) of ether-based (1 M LiTFSI in DME/DOL (1:1 by volume)) or LP30 (1 M $LiPF_6$ in EC/DMC (1:1 by volume)) electrolyte was added. All measurements were performed at constant laboratory temperature (22 ± 2 °C). The capacity and long-term stability of the cells was characterized by galvanostatic cycling with a BASYTEC CTS cell test system. The Li–S cells with S@CTF cathodes were operated at a constant rate of C/10 (1 C = 1672 mA g_{sulfur}^{-1}). The reference cells with the pure CTF material were characterized by using a constant current density of 0.10 mA cm^{-2}. The coulombic efficiency (CE) was calculated by dividing the discharge (lithiation) capacity by the charge (delithiation) capacity. In order to compare both electrolyte systems with the results of Fanous *et al.*[20] and to avoid the depletion of LiTFSI and DOL, all galvanostatic cycling tests were operated in a voltage range of 1.20–3.00 V vs. Li/Li^+ due to the stability window of LP30.[45]

Acknowledgements

This work has received funding from the Federal Ministry of Education and Research (BMBF), support code 03XP0030 ("StickLiS"). We would like to thank Peter Schützendübe and Gunther Richter, MPI-IS, for performing the XPS measurements.

Conflict of Interest

The authors declare no conflict of interest.

Keywords: lithium-sulfur battery · cathode material · covalent triazine framework · covalently bound sulfur · mechanistic insights

[1] P. G. Bruce, S. A. Freunberger, L. J. Hardwick, J.-M. Tarascon, *Nat. Mater.* **2011**, *11*, 19–29.
[2] G. Li, Z. Chen, J. Lu, *Chem* **2018**, *4*, 3–7.
[3] a) X. Ji, L. F. Nazar, *J. Mater. Chem.* **2010**, *20*, 9821–9826; b) A. Fotouhi, D. Auger, L. O'Neill, T. Cleaver, S. Walus, *Energies* **2017**, *10*, 1937.
[4] R. Kumar, J. Liu, J.-Y. Hwang, Y.-K. Sun, *J. Mater. Chem. A* **2018**, *6*, 11582–11605.
[5] T. Cleaver, P. Kovacik, M. Marinescu, T. Zhang, G. Offer, *J. Electrochem. Soc.* **2018**, *165*, A6029-A6033.
[6] R. Cao, W. Xu, D. Lv, J. Xiao, J.-G. Zhang, *Adv. Energy Mater.* **2015**, *5*, 1402273.
[7] a) M. Wild, L. O'Neill, T. Zhang, R. Purkayastha, G. Minton, M. Marinescu, G. J. Offer, *Energy Environ. Sci.* **2015**, *8*, 3477–3794; b) M. Safari, C. Y. Kwok, L. F. Nazar, *ACS Cent. Sci.* **2016**, *2*, 560–568; c) M. Marinescu, L. O'Neill, T. Zhang, S. Walus, T. E. Wilson, G. J. Offer, *J. e Electrochem. Soc.* **2018**, *165*, A6108–A6118.
[8] L. Borchardt, M. Oschatz, S. Kaskel, *Chem. Eur. J.* **2016**, *22*, 7324–7351.
[9] S. Dörfler, P. Strubel, T. Jaumann, E. Troschke, F. Hippauf, C. Kensy, A. Schökel, H. Althues, L. Giebeler, S. Oswald, et al., *Nano Energy* **2018**, *54*, 116–128.
[10] C. Schneidermann, C. Kensy, P. Otto, S. Oswald, L. Giebeler, D. Leistenschneider, S. Grätz, S. Dörfler, S. Kaskel, L. Borchardt, *ChemSusChem* **2019**, *12*, 310–319.
[11] C. Kensy, P. Härtel, J. Maschita, S. Dörfler, B. Schumm, T. Abendroth, H. Althues, B. V. Lotsch, S. Kaskel, *Carbon* **2020**, *161*, 190–197.
[12] a) Z. Wei Seh, W. Li, J. J. Cha, G. Zheng, Y. Yang, M. T. McDowell, P.-C. Hsu, Y. Cui, *Nat. Commun.* **2013**, *4*, 1331; b) Q. Pang, D. Kundu, M. Cuisinier, L. F. Nazar, *Nat. Commun.* **2014**, *5*, 4759; c) Z. Li, H. Jiang, N.-C. Lai, T. Zhao, Y.-C. Lu, *Chem. Mater.* **2019**, *31*, 10186–10196.
[13] a) S.-E. Cheon, J.-H. Cho, K. S. Ko, C.-W. Kwon, D.-R. Chang, H.-T. Kim, S.-W. Kim, *J. Electrochem. Soc.* **2002**, *149*, A1437–A1441; b) M. J. Lacey, F. Jeschull, K. Edström, D. Brandell, *Chem. Commun.* **2013**, *49*, 8531–8533.
[14] T. Yim, M.-S. Park, J.-S. Yu, K. J. Kim, K. Y. Im, J.-H. Kim, G. Jeong, Y. N. Jo, S.-G. Woo, K. S. Kang, et al., *Electrochim. Acta* **2013**, *107*, 454–460.
[15] S. Xin, L. Gu, N.-H. Zhao, Y.-X. Yin, L.-J. Zhou, Y.-G. Guo, L.-J. Wan, *J. Am. Chem. Soc.* **2012**, *134*, 18510–18513.
[16] a) Z. Li, L. Yuan, Z. Yi, Y. Sun, Y. Liu, Y. Jiang, Y. Shen, Y. Xin, Z. Zhang, Y. Huang, *Adv. Energy Mater.* **2014**, *4*, 1301473; b) J. T. Lee, Y. Zhao, S. Thieme, H. Kim, M. Oschatz, L. Borchardt, A. Magasinski, W.-I. Cho, S. Kaskel, G. Yushin, *Adv. Mater.* **2013**, *25*, 4573–4579.
[17] X. Li, M. Banis, A. Lushington, X. Yang, Q. Sun, Y. Zhao, C. Liu, Q. Li, B. Wang, W. Xiao, et al., *Nat. Commun.* **2018**, *9*, 4509.
[18] J. Fanous, M. Wegner, J. Grimminger, Ä. Andresen, M. R. Buchmeiser, *Chem. Mater.* **2011**, *23*, 5024–5028.
[19] J. Fanous, M. Wegner, M. B. M. Spera, M. R. Buchmeiser, *J. Electrochem. Soc.* **2013**, *160*, A1169–A1170.
[20] S. Zhang, *Energies* **2014**, *7*, 4588–4600.
[21] a) J. Wang, J. Yang, C. Wan, K. Du, J. Xie, N. Xu, *Adv. Funct. Mater.* **2003**, *13*, 487–492; b) G.-B. Cho, H.-B. Park, J.-S. Jeong, M.-R. Chae, Y.-M. Im, L. Han-Gyeol, P. Sang-Hui, K.-W. Kim, *J. Nanosci. Nanotechnol.* **2018**, *18*, 6431–6436; c) C. J. Kuo, M. A. Weret, H. Hung, M. Tsai, C. Huang, W. Su, B. Hwang, *J. Power Sources* **2019**, *412*, 670–676; d) Y. Liu, A. K. Haridas, Y. Lee, K.-K. Cho, J.-H. Ahn, *Appl. Surf. Sci.* **2019**, *472*, 135–142; e) W. Wang, Z. Cao, G. A. Elia, Y. Wu, W. Wahyudi, E. Abou-Hamad, A.-H. Emwas, L. Cavallo, L.-J. Li, J. Ming, *ACS Energy Lett.* **2018**, *3*, 2899–2907.
[22] Y. Li, Q. Zeng, I. R. Gentle, D.-W. Wang, *J. Mater. Chem. A* **2017**, *5*, 5460–5465.
[23] S. Warneke, R. K. Zenn, T. Lebherz, K. Müller, A. Hintennach, U. Starke, R. E. Dinnebier, M. R. Buchmeiser, *Adv. Sustainable Syst.* **2018**, *2*, 1700144.
[24] T. Lebherz, M. Frey, A. Hintennach, M. R. Buchmeiser, *RSC Adv.* **2019**, *9*, 7181–7188.
[25] a) H. Liao, H. Wang, H. Ding, X. Meng, H. Xu, B. Wang, X. Ai, C. Wang, *J. Mater. Chem. A* **2016**, *4*, 7416–7421; b) L. Li, W. Fang, P. Zhang, J. Bi, Y. He, J. Wang, W. Su, *J. Mater. Chem. A* **2016**, *4*, 12402–12406.
[26] F. Xu, S. Yang, G. Jiang, Q. Ye, B. Wei, H. Wang, *ACS Appl. Mater. Interfaces* **2017**, *9*, 37731–37738.
[27] Z. Cheng, H. Pan, H. Zhong, Z. Xiao, X. Li, R. Wang, *Adv. Funct. Mater.* **2018**, *28*, 1707597.
[28] J. Xu, F. Yu, J. Hua, W. Tang, C. Yang, S. Hu, S. Zhao, X. Zhang, Z. Xin, D. Niu, *Chem. Eng. J.* **2019**, 123694.
[29] Q. X. Shi, H. J. Pei, N. You, J. Wu, X. Xiang, Q. Xia, X. L. Xie, S. B. Jin, Y. S. Ye, *Chem. Eng. J.* **2019**, *375*, 121977.
[30] D. -G Wang, L. Tan, H. Wang, M. Song, J. Wang, G. -C Kuang, *ChemElectroChem* **2019**, *6*, 2777–2781.
[31] R. Guan, L. Zhong, S. Wang, D. Han, M. Xiao, L. Sun, Y. Meng, *ACS Appl. Mater. Interfaces* **2020**, *12*, 8296–8305.
[32] P. Kuhn, M. Antonietti, A. Thomas, *Angew. Chem. Int. Ed.* **2008**, *47*, 3450–3453; *Angew. Chem.* **2008**, *120*, 3499–3502.
[33] E. Troschke, S. Grätz, L. Borchardt, D. Haubold, I. Senkovska, A. Eychmueller, S. Kaskel, *Microporous Mesoporous Mater.* **2017**, *239*, 190–194.
[34] S. N. Talapaneni, T. H. Hwang, S. H. Je, O. Buyukcakir, J. W. Choi, A. Coskun, *Angew. Chem. Int. Ed.* **2016**, *55*, 3106–3111; *Angew. Chem.* **2016**, *128*, 3158–3163.
[35] S. Royuela, J. Almarza, M. J. Mancheño, J. C. Pérez-Flores, E. G. Michel, M. M. Ramos, F. Zamora, P. Ocón, J. L. Segura, *Chem. Eur. J.* **2019**, *25*, 12394–12404.
[36] a) P. Kuhn, A. Thomas, M. Antonietti, *Macromolecules* **2009**, *42*, 319–326; b) E. Troschke, S. Grätz, T. Lübken, L. Borchardt, *Angew. Chem. Int. Ed.* **2017**, *56*, 6859–6863; *Angew. Chem.* **2017**, *129*, 6963–6967.
[37] P. Kuhn, A. Forget, D. Su, A. Thomas, M. Antonietti, *J. Am. Chem. Soc.* **2008**, *130*, 13333–13337.
[38] F. Hippauf, W. Nickel, G.-P. Hao, K. Schwedtmann, L. Giebeler, S. Oswald, L. Borchardt, S. Doerfler, J. J. Weigand, S. Kaskel, *Adv. Mater. Interfaces* **2016**, *3*, 1600508.
[39] J. Yoo, S.-J. Cho, G. Y. Jung, S. H. Kim, K.-H. Choi, J.-H. Kim, C. K. Lee, S. K. Kwak, S.-Y. Lee, *Nano Lett.* **2016**, *16*, 3292–3300.
[40] X. Jiang, P. Wang, J. Zhao, *J. Mater. Chem. A* **2015**, *3*, 7750–7758.
[41] K. A. See, S. Hug, K. Schwinghammer, M. A. Lumley, Y. Zheng, J. M. Nolt, G. D. Stucky, F. Wudl, B. V. Lotsch, R. Seshadri, *Chem. Mater.* **2015**, *27*, 3821–3829.
[42] a) L. Hao, J. Ning, B. Luo, B. Wang, Y. Zhang, Z. Tang, J. Yang, A. Thomas, L. Zhi, *J. Am. Chem. Soc.* **2015**, *137*, 219–225; b) K. Sakaushi, G. Nickerl, F. M. Wisser, D. Nishio-Hamane, E. Hosono, H. Zhou, S. Kaskel, J. Eckert, *Angew. Chem. Int. Ed.* **2012**, *51*, 7850–7854; *Angew. Chem.* **2012**, *124*, 7972–7976.
[43] J. Rouquerol, P. Llewellyn, F. Rouquerol, *Stud. Surf. Sci. Catal.* **2007**, *160*, 49–56.
[44] E. Troschke, "Novel Synthetic Pathways for Tailored Covalent Triazine Frameworks with Catalytic and Electrochemical Applications", can be found under https://nbn-resolving.org/urn:nbn:de:bsz:14-qucosa2-323500, **2018**.
[45] S. Thieme, J. Brückner, I. Bauer, M. Oschatz, L. Borchardt, H. Althues, S. Kaskel, *J. Mater. Chem. A* **2013**, *1*, 9225–9234.
[46] V. Sharova, A. Moretti, T. Diemant, A. Varzi, R. J. Behm, S. Passerini, *J. Power Sources* **2018**, *375*, 43–52.
[47] P. Kuhn, A. Forget, J. Hartmann, A. Thomas, M. Antonietti, *Adv. Mater.* **2009**, *21*, 897–901.
[48] M. Cuisinier, P.-E. Cabelguen, S. Evers, G. He, M. Kolbeck, A. Garsuch, T. Bolin, M. Balasubramanian, L. F. Nazar, *J. Phys. Chem. Lett.* **2013**, *4*, 3227–3232.
[49] J. F. Moulder, W. F. Stickle, P. E. Sobol, *Handbook of X-ray photoelectron spectroscopy. A reference book of standard spectra for identification and interpretation of XPS data*, Physical Electronics, Inc, Eden Prairie, Minn., **1995**.
[50] C. H. Chang, *Carbon* **1981**, *19*, 175–186.

[51] T. Grzybek, R. Pietrzak, H. Wachowska, *Fuel Process. Technol.* **2002**, *77–78*, 1–7.
[52] W. Kiciński, M. Szala, M. Bystrzejewski, *Carbon* **2014**, *68*, 1–32.
[53] a) S. Wei, L. Ma, K. E. Hendrickson, Z. Tu, L. A. Archer, *J. Am. Chem. Soc.* **2015**, *137*, 12143–12152; b) L. Wang, X. He, J. Li, J. Gao, J. Guo, C. Jiang, C. Wan, *J. Mater. Chem.* **2012**, *22*, 22077–22081.
[54] S. Thieme, J. Brückner, A. Meier, I. Bauer, K. Gruber, J. Kaspar, A. Helmer, H. Althues, M. Schmuck, S. Kaskel, *J. Mater. Chem. A* **2015**, *3*, 3808–3820.
[55] J. Scheers, S. Fantini, P. Johansson, *J. Power Sources* **2014**, *255*, 204–218.
[56] a) M. Cuisinier, C. Hart, M. Balasubramanian, A. Garsuch, L. F. Nazar, *Adv. Energy Mater.* **2015**, *5*, 1401801; b) C. Barchasz, F. Molton, C. Duboc, J.-C. Leprêtre, S. Patoux, F. Alloin, *Anal. Chem.* **2012**, *84*, 3973–3980.
[57] D.-W. Wang, G. Zhou, F. Li, K.-H. Wu, G. Q. M. Lu, H.-M. Cheng, I. R. Gentle, *Phys. Chem. Chem. Phys.* **2012**, *14*, 8703–8710.
[58] S. S. Zhang, *Electrochim. Acta* **2012**, *70*, 344–348.
[59] M. J. Lacey, A. Yalamanchili, J. Maibach, C. Tengstedt, K. Edström, D. Brandell, *RSC Adv.* **2016**, *6*, 3632–3641.
[60] E. Peled, S. Menkin, *J. Electrochem. Soc.* **2017**, *164*, A1703–A1719.
[61] S. S. Zhang, *J. Power Sources* **2016**, *322*, 99–105.
[62] J. Brückner, S. Thieme, H. T. Grossmann, S. Dörfler, H. Althues, S. Kaskel, *J. Power Sources* **2014**, *268*, 82–87.
[63] Q. Pang, X. Liang, C. Y. Kwok, L. F. Nazar, *Nat. Energy* **2016**, *1*, 652.
[64] S. H. Je, H. J. Kim, J. Kim, J. W. Choi, A. Coskun, *Adv. Funct. Mater.* **2017**, *114*, 1703947.
[65] C. Liang, N. J. Dudney, J. Y. Howe, *Chem. Mater.* **2009**, *21*, 4724–4730.

Manuscript received: March 25, 2020
Revised manuscript received: April 22, 2020
Accepted manuscript online: April 29, 2020
Version of record online: June 8, 2020